PNAS RESEARCH ARTICLE | BIOPHYSICS AND COMPUTATIONAL BIOLOGY

A fine balance of hydrophobic-electrostatic communication pathways in a pH-switching protein

Duncan W. S. MacKenzie[a], Anna Schaefer[a,1], Julia Steckner[a,1], Christopher A. Leo[a], Dalia Naser[a], Efrosini Artikis[b,2], Aron Broom[a], Travis Ko[a], Purnank Shah[a], Mikaela Q. Ney[a], Elisa Tran[a], Martin T. J. Smith[a], Brian Fuglestad[c,3], A. Joshua Wand[c,4], Charles L. Brooks III[b], and Elizabeth M. Meiering[a,5]

Edited by William DeGrado, University of California, San Francisco, CA; received October 27, 2021; accepted March 29, 2022

Allostery is the phenomenon of coupling between distal binding sites in a protein. Such coupling is at the crux of protein function and regulation in a myriad of scenarios, yet determining the molecular mechanisms of coupling networks in proteins remains a major challenge. Here, we report mechanisms governing pH-dependent myristoyl switching in monomeric hisactophilin, whereby the myristoyl moves between a sequestered state, i.e., buried within the core of the protein, to an accessible state, in which the myristoyl has increased accessibility for membrane binding. Measurements of the pH and temperature dependence of amide chemical shifts reveal protein local structural stability and conformational heterogeneity that accompany switching. An analysis of these measurements using a thermodynamic cycle framework shows that myristoyl-proton coupling at the single-residue level exists in a fine balance and extends throughout the protein. Strikingly, small changes in the stereochemistry or size of core and surface hydrophobic residues by point mutations readily break, restore, or tune myristoyl switch energetics. Synthesizing the experimental results with those of molecular dynamics simulations illuminates atomistic details of coupling throughout the protein, featuring a large network of hydrophobic interactions that work in concert with key electrostatic interactions. The simulations were critical for discerning which of the many ionizable residues in hisactophilin are important for switching and identifying the contributions of nonnative interactions in switching. The strategy of using temperature-dependent NMR presented here offers a powerful, widely applicable way to elucidate the molecular mechanisms of allostery in proteins at high resolution.

allostery | NMR temperature dependence | switch | pH dependence | myristoylation

Significance

Accurately capturing the intricate interaction networks that control protein allostery is a central goal in protein science. We present a means to determine these networks by high-resolution NMR difference and coupling measurements, illustrated for pH-dependent myristoyl switching in hisactophilin. Integrated temperature and pH dependence of protein amide NMR synergistic with molecular dynamics (MD) simulations resolves nuances of a proteinwide interaction network, with proton binding by histidines in balance with extensive core and surface hydrophobic interactions. Analysis of mutant proteins demonstrates how this web of switching interactions can be broken, restored, and tuned. Thus, high-sensitivity NMR may be used to define the intricacies of interaction networks in a wide variety of protein and peptide systems.

Protein allostery is the process whereby ligand binding at one site in the protein affects binding at another functional site, allowing for regulation of the corresponding function. Despite the centrality of allostery to a tremendous range of protein function, defining the molecular mechanisms of allostery and the accompanying energetics remains a central challenge in biochemistry (1, 2). The challenge arises from the multitude of intra- and intermolecular interactions in proteins and their ligands, which affect one another in intricate ways that remain experimentally obscure and hard to predict.

Here, we focus on proton binding–regulated functional myristoyl switching in hisactophilin, an actin binding protein from *Dictyostelium discoideum* containing 31 histidine residues (Fig. 1 *A* and *B*) (3, 4). Myristoylation is the covalent attachment of a C14 fatty acyl chain to an N-terminal glycine in a protein. Allosteric control of switching of the state of the myristoyl plays a vital role in a wide variety of regulated protein-membrane and protein-protein interactions (5–7). For example, myristoyl switching is involved in natural processes such as chemotaxis and response to osmotic stress by hisactophilin (8), light signal transduction in the retina by recoverin (5), and disease processes in cancer and viral infections (9–11). Hisactophilin exemplifies reversible, ligand binding–regulated, myristoyl switching; specifically, binding of ∼1.5 protons causes a switch from a sequestered state, in which the myristoyl is buried within the core of the protein, to an accessible state, in which the myristoyl has increased accessibility for membrane binding (12) (Fig. 1*B*). While coarse-grained modeling has implicated nonnative hydrophobic and histidine interactions in switching, the molecular details are still unknown (13).

Solution NMR is a powerful means to characterize different states of proteins. In particular, the temperature dependencies of amide proton (^{1}H) chemical shifts provide valuable probes of hydrogen bonding and temperature-dependent changes in local protein structure, as well as conformational sampling of distinct near-native states (14–18). Interestingly, the well-established relationships of amide temperature coefficients (TCs) with hydrogen bonding were extended to a more general observation of TCs reporting on protein structural stability (18, 19). However, as the many intra- and

The authors declare no competing interest.

This article is a PNAS Direct Submission.

[1]A.S. and J.S. contributed equally to this work.

[2]Present address: Laboratory of Persistent Viral Diseases, Rocky Mountain Laboratories, National Institute of Allergy and Infectious Diseases, National Institutes of Health, Hamilton, MT 59840.

[3]Present address: Department of Chemistry, Virginia Commonwealth University, Richmond, VA 23284.

[4]Present address: Department of Biochemistry and Biophysics, Texas A&M University, College Station, TX 77843.

[5]To whom correspondence may be addressed. Email: meiering@uwaterloo.ca.

This article contains supporting information online at http://www.pnas.org/lookup/suppl/doi:10.1073/pnas.2119686119/-/DCSupplemental.

Published June 22, 2022.

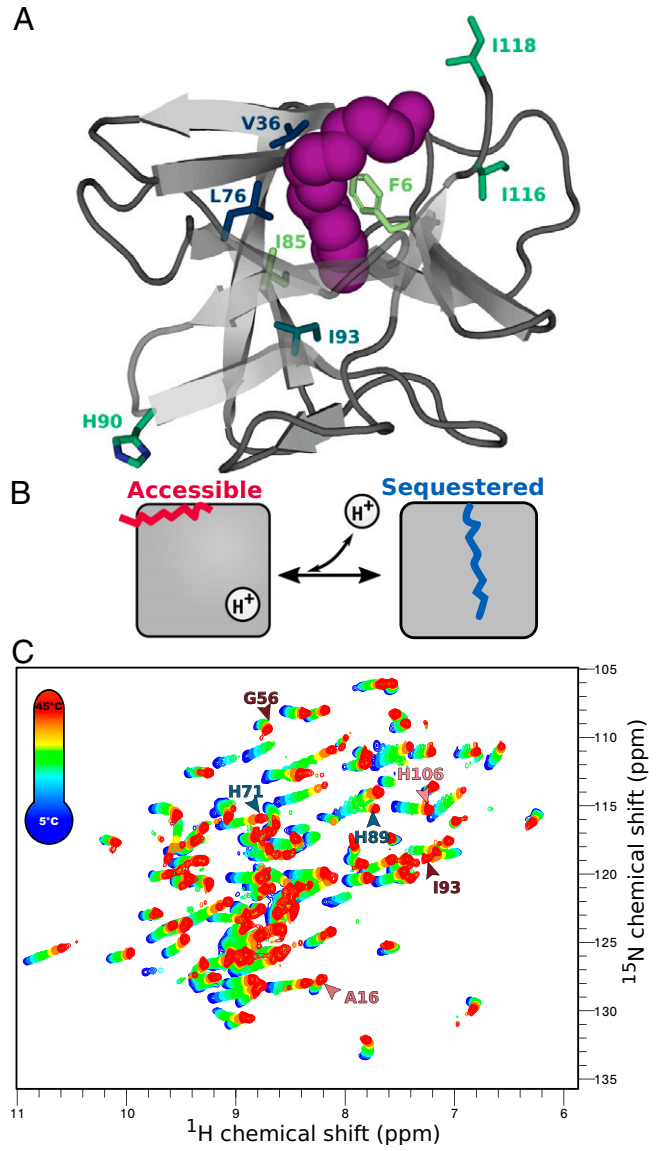

Fig. 1. Hisactophilin myristoyl pH switch analyzed by NMR. (*A*) Structure of myristoylated hisactophilin. Structure model based on the NMR structure at pH 6.8 (PDB: 1HCD), near the midpoint of switching, with myristoyl (magenta spheres) modeled based on NOE restraints (12). Side chains mutated in this study are shown as sticks. Solvent-exposed residues H90 (in a turn), I116, and I118 (C terminus) are green. F6 and I85 in the bottom β-barrel layer are light green, V36 and L76 in the middle hydrophobic layer of the β-barrel are dark blue, and I93 in the upper β-barrel layer is turquoise (14). (*B*) Schematic of the hisactophilin pH-myristoyl switch. Myristoyl (wavy line) is sequestered in the protein (gray square) at high pH (*Right*) and switches to a state with increased myristoyl accessibility upon proton binding at lower pH (*Left*). A summary of backbone amide resonance assignments for WT hisactophilin has been submitted to BMRB (*SI Appendix, Supplementary Methods*). (*C*) Variable-temperature ^{1}H-^{15}N HSQC spectra of myristoylated hisactophilin at pH 6.2. Spectra were taken at 5 to 45 °C in 5 °C increments. ppm, parts per million.

intermolecular contributions to chemical shift vary in complex ways with temperature, a quantitative structural interpretation of TCs has remained elusive. Recent studies in our group and others have shown how the complexities of amide temperature dependencies may be simplified by comparing related protein variants, yielding nuanced information on changes in structural stability and sampling of alternative states significant for natural function, disease, drug discovery, and materials (6, 16–26).

Here, we report how differences in temperature and pH dependence of amide chemical shifts, and a combined analysis using a thermodynamic cycle framework, discern the molecular underpinnings of allosteric myristoyl switching in hisactophilin. Applying the NMR experiments with site-directed mutagenesis and computational modeling reveals an extensive network of interacting residues, including the major hydrophobic core coordinated with surface electrostatic interactions of key histidines. Conservative changes to buried and exposed hydrophobic groups alter a cascade of interactions that easily tip the fine balance of switching states and thus readily break, repair, or modulate pH-dependent myristoyl switching.

Results and Discussion

Amide TCs Show Extensive Changes in Local Protein Stability during Switching. The linear temperature dependencies of backbone amide proton chemical shifts, or TCs, are sensitive reporters of local protein structural stability (16–18). To examine how myristoyl switching impacts local stability in wild-type (WT) hisactophilin, amide chemical shifts were measured using ^{1}H-^{15}N heteronuclear single quantum correlation (HSQC) spectra acquired as a function of temperature at pH 7.7 and 6.2, i.e., values above and below 6.95, the midpoint of switching (pK_{switch}) (Fig. 1*C*). At pH 7.7, the myristoyl is mainly sequestered within the protein (the sequestered state), while at pH 6.2, it has increased accessibility for membrane binding (the accessible state) (12) (assignments deposited in the BMRB (Biological Magnetic Resonance Bank), deposition numbers in *SI Appendix, Supplementary Methods*). In general, amides in more stable structures exhibit smaller decreases in chemical shifts with increasing temperature (*SI Appendix*, Fig. S1 and S2), as is evident for residues in β strands (e.g., A16 and G56) versus ones in flexible loops (e.g., H89 and H106) (Fig. 2 *A* and *B* and *SI Appendix*, Tables S3 and S4) (14, 15, 27). To assess differences in stability when the myristoyl switches from accessible to sequestered, we measured the change in TC from pH 6.2 to 7.7 ($\Delta TC_{Seq\text{-}Acc} = TC_{pH\ 7.7} - TC_{pH\ 6.2}$) (Fig. 2 *C*–*E*). The number of residues that were stabilized in the sequestered or accessible states were similar but distributed across different parts of the protein. These results indicate extensive differences in local stability throughout the protein between the two states of the switch.

Myristoyl-H^{+} Coupling Distributed throughout WT Is Disrupted in Broken-Switch Mutants. To establish the molecular details of the switching mechanism, we assessed the coupling between myristoyl switching and proton binding ($Coupling_{Myr\text{-}H+}$) on a per-residue basis by applying thermodynamic cycle analysis to WT amide TCs (Fig. 3*A*). This analysis of TCs is conceptually similar to established methods whereby coupling between two groups is determined by systematically altering them individually and together (e.g., by mutagenesis or addition of a ligand) (*SI Appendix*, Fig. S3) and observing the resulting changes in global protein stability (12, 28–30). This cycle analysis allows unrelated interactions to be subtracted out so that specific interactions can be examined. The TC cycle has the important advantage of assessing the myristoyl-proton coupling at many sites concurrently, giving a unique high-resolution view.

For the cycle analysis, we define myristoyl-H^{+} coupling as the difference in amide structural stability in myristoylated (TC_{myr}) relative to nonmyristoyled (TC_{non}) WT at pH 7.7 relative to pH 6.2 (Fig. 3*A* and *SI Appendix*, Table S3):

$$Coupling_{Myr-H+} = \left(TC_{myr} - TC_{non}\right)_{pH7.7} - \left(TC_{myr} - TC_{non}\right)_{pH6.2}.$$

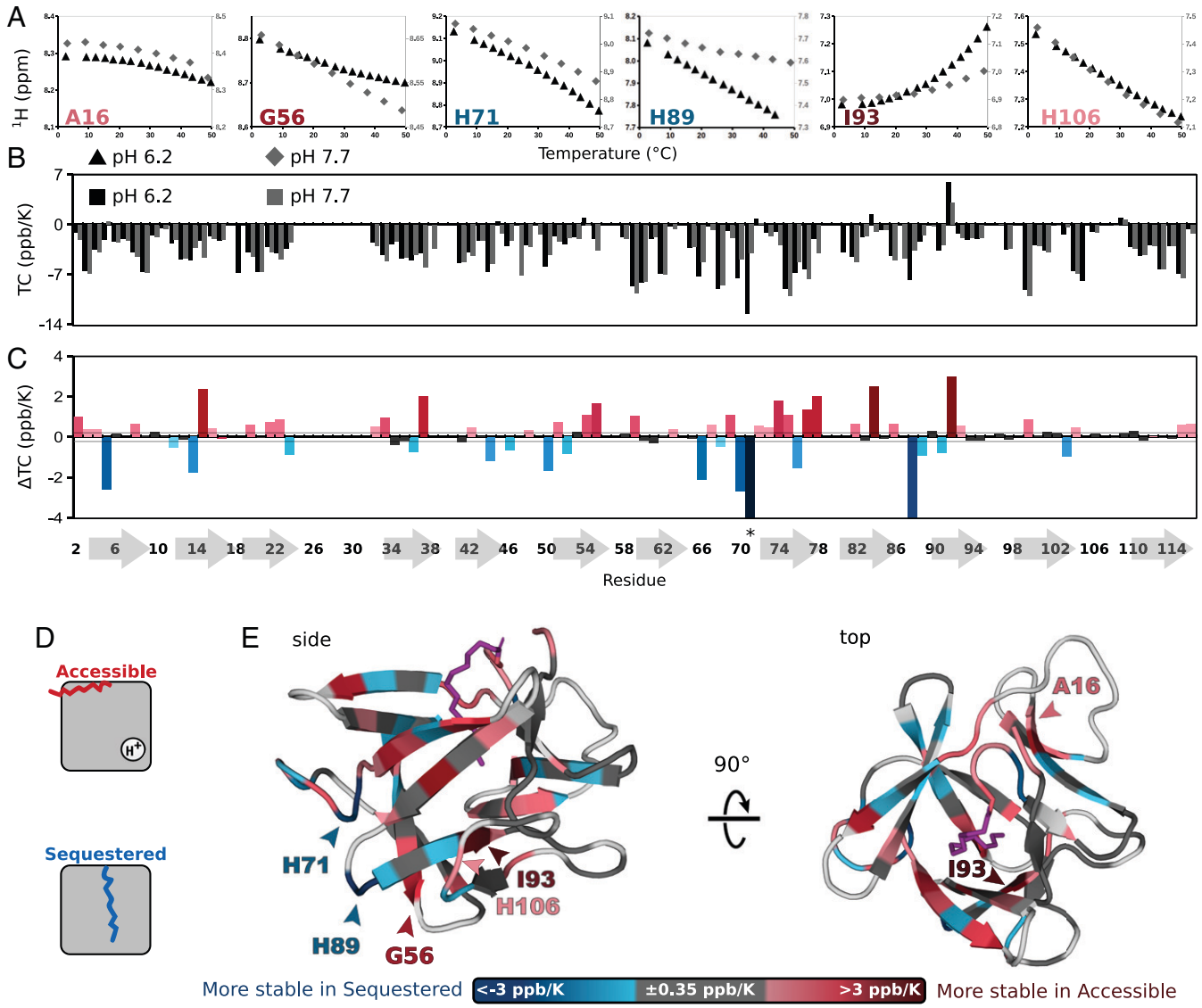

Fig. 2. Amide TCs of myristoylated and nonmyristoylated WT hisactophilin. (*A*) ^{1}H chemical shift versus temperature for selected amides in myristoylated hisactophilin at pH 6.2 (black triangles) and pH 7.7 (gray diamonds). A smaller TC (i.e., a smaller decrease in chemical shift with increasing temperature) indicates greater structural stability (15, 16). (*B*) TCs (in parts per billion per Kelvin [ppb/K]) from linear fits of the data for each residue in WT hisactophilin at pH 6.2 (black) and pH 7.7 (gray). (*C*) Differences in TC at pH 7.7 relative to pH 6.2 ($\Delta TC_{Seq\text{-}Acc} = TC_{pH7.7} - TC_{pH6.2}$). The difference provides a measure of the change in local structural stability in the sequestered versus accessible state. For example, TCs suggest that G56 and I93 are more stable in the accessible state, H71 and H89 are more stable in the sequestered state, and there is very little change for A16 and H106. (*D*) Switching scheme showing accessible myristoyl at low pH (proton bound) and sequestered myristoyl at high pH (no proton bound). (*E*) Hisactophilin structure colored according to the differences in TC at pH 7.7 relative to pH 6.2. TC values are given in *SI Appendix*, Tables S1–S3.

A positive coupling value suggests the myristoyl increases local protein stability at pH 6.2, i.e., in the presence of bound H^+ (the accessible state); conversely, a negative value indicates the myristoyl increases stability at pH 7.7, in the absence of bound H^+ (the sequestered state). Strikingly, both positive and negative coupling are abundantly apparent throughout the WT structure, indicating a highly distributed balance of local stability favoring each state (Fig. 3*B*).

We then applied the TC cycle coupling analysis to two hydrophobic core mutants of hisactophilin, I85L and I85L/F6L/I93L (LLL). These mutants were chosen based on previous chemical denaturation experiments (which measure global protein stability) indicating that myristoyl-H^+ switching is broken. While in principle the mutations may alter what conformations are accessible to the protein, the data indicate the mutants predominantly populate just one state, resembling either accessible (I85L) or sequestered (LLL) (*SI Appendix*, Tables S5 and S6) (12, 13, 30). For the point mutant I85L, myristoylation confers a small increase in global protein stability at pH 6.2, which does not increase significantly with increased pH; the small stabilization (comparable to WT at pH 6.2) and computational modeling indicate that switching is broken so that the protein mainly populates a state resembling accessible. In contrast, the triple-mutant LLL is broken to favor a state resembling sequestered, with the myristoyl conferring a large increase in stability at all pH levels (similar to WT at pH 7.7) and remaining sequestered within the expanded cavity in the protein (Fig. 2). The two broken-switch mutants provide key controls to confirm that TC analysis identifies changes between the accessible and the sequestered states in WT. In agreement with the global coupling measurements, the extensive network of positive and negative Myr-H^+ coupling observed for WT is strikingly diminished in both I85L and LLL (Fig. 3). These results are particularly notable given that the mutant switches are broken

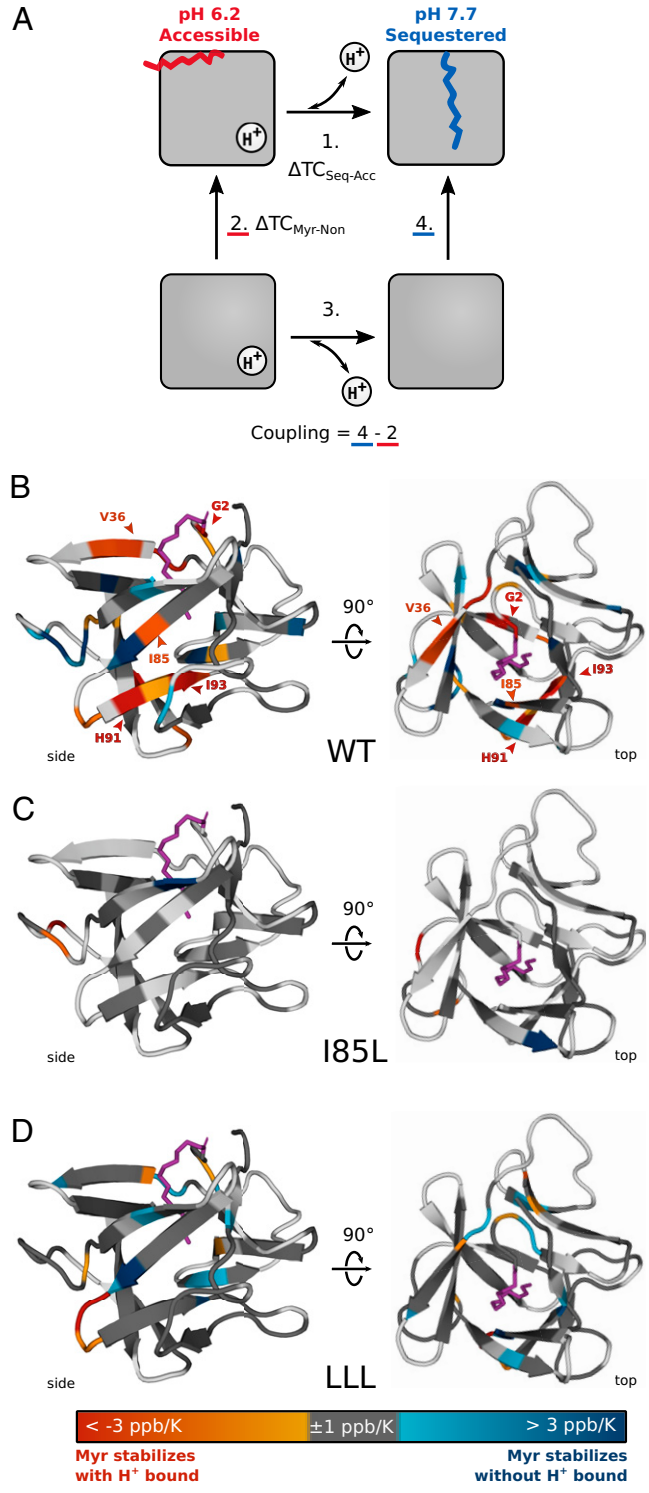

Fig. 3. TC cycle analyses show the extensive Myr-H^+ coupling network in WT is diminished in broken-switch I85L and LLL hisactophilin. (*A*) Cycle analysis for amide TCs. The cycle takes the differences between myristoylated hisactophilin (top gray squares with a wavy line) and nonmyristoyled hisactophilin (bottom gray squares), in the presence (pH 6.2) or absence (pH 7.7) of bound protons. The myristoyl-H^+ coupling for individual amides was calculated as $\text{Coupling}_{\text{Myr-H+}} = (\text{TC}_{\text{myr}} - \text{TC}_{\text{non}})_{\text{pH7.7}} - (\text{TC}_{\text{myr}} - \text{TC}_{\text{non}})_{\text{pH6.2}} = 4–2 = 1–3$ (raw values for calculation are in *SI Appendix*, Tables S1 and S2). Values for $\text{Coupling}_{\text{Myr-H+}}$ are mapped onto a model of the structure of myristoylated hisactophilin at pH 6.8 (12), shown viewed from the side and from the top, for (*B*) WT, (*C*) I85L, and (*D*) LLL. The coupling values are also shown as bar graphs in *SI Appendix*, Fig. S5. WT exhibits extensive positive (red) and negative (blue) coupling, indicating a balance of interactions favoring accessible or sequestered, respectively. Coupling is greatly diminished in the broken-switch mutants.

such that they predominantly populate different states with considerably different stabilities and provide strong support for the identification of coupling using TC cycles.

Thermodynamic cycle analysis of protein chemical denaturation is a well-established approach to measuring pairwise coupling between bound ligands and/or individual residues in proteins (28, 30). This approach requires experiments on separate double-mutant cycles for each interacting pair to obtain a high-resolution view of coupling. Attractive aspects of the alternative TC cycles described herein are the facile analysis of many residues simultaneously, without needing to make and analyze many mutants. In addition, the cycle framework can simplify and provide deeper interpretation of the TC data.

Population of Alternative States by WT Is Much Reduced in Broken-Switch Mutants. Beyond TCs, subtle nonlinearities in the temperature dependence of amide ^{1}H chemical shifts provide additional valuable information as they report on the population of alternative states in proteins, as has been observed in a variety of binding proteins and enzymes (6, 17, 18, 31–33). This curvature is detected through analysis of the observed chemical shift relative to the line of best fit of a TC, and the sign of the curve (concave or convex) generally correlates with the amide proton chemical shift relative to the random coil (17, 33). Many more amides exhibit curved temperature dependencies in myristoylated compared to nonmyristoylated WT hisactophilin (Fig. 4 and *SI Appendix*, Tables S1 and S2). The myristoyl-induced effects observed in WT are again markedly attenuated, but not eliminated, in the mutants. Intriguingly, the remaining curvature is modestly higher for I85L than for LLL, perhaps due to the unstable nature of the accessible myristoyl in I85L still seeking hydrophobic burial compared to a more stable sequestered state in LLL (*SI Appendix*, Fig. S5 and Table S2). Thus, curvature provides a sensitive readout of significant remaining dynamics and extends the view of changes in function beyond that given by global stability change. For WT hisactophilin, the switching free-energy difference between myristoyl sequestered and accessible states, ΔG_{Switch}, of 2.0 kcal mol^{-1} (12) is in a range where curvature may be most readily detectable (17, 27, 31, 33, 34). Despite this moderate energy difference, many residues throughout the protein participate in switching.

pH Dependence of Amide Chemical Shifts Show that Extensive Changes in pK_{app} Accompany Switching. To examine how ionizable groups contribute to switching, we also measured the pH dependence of ^{1}H-^{15}N HSQC spectra for myristoylated compared to nonmyristoylated WT, I85L, and LLL hisactophilin (*SI Appendix*, Fig. S6). The nonmyristoylated form may serve as a model for the protein when the myristoyl is fully exposed and no longer in its binding pocket (12, 13), which occurs during functional membrane binding by hisactophilin (4). In these experiments, amide apparent pK_a (pK_{app}) values serve as indirect reporters of the ionizable groups that influence the amide environments (12). Previous studies showed the pH switch for WT from sequestered to accessible myristoyl is coupled to the net binding of ~1.5 H^+ due to an increase in pK_a from 6 to 6.5 to from ~7 to 7.6 involving multiple (at least two) ionizable groups (12). Owing to the complex and extensive changes in amide pK_{app} values throughout the protein (*SI Appendix*, Fig. S6), the specific ionizable groups could not be determined from among the many possibilities (31 His, 6 Asp, and 7 Glu). In I85L and LLL, the changes in pK_{app} upon myristoylation are largely abrogated, again in agreement with their broken

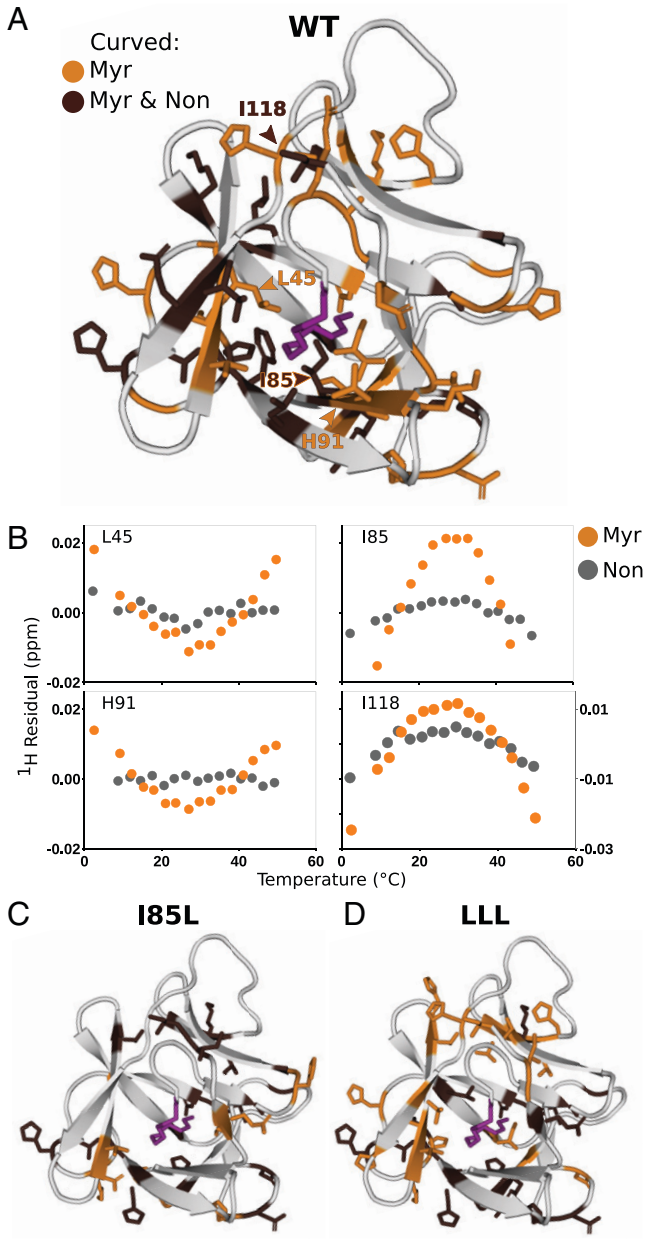

Fig. 4. Curved temperature dependencies implicating the existence of multiple conformations in myristoylated (Myr) WT are decreased in the broken-switch mutants. (*A*) Residues exhibiting significant residual amide chemical shift curvature with temperature in Myr WT hisactophilin only (orange) or in both Myr and nonmyristoylated (Non) WT (brown) at pH 6.2. Only residuals that deviate from linearity at a stringent significance cutoff of $P = 0.01$ are shown (*SI Appendix*, Table S1 and S2 and *Supplementary Methods*). (*B*) Representative residual amide chemical shifts versus temperature for WT. (*C* and *D*) Ribbons for I85L and LLL mutants, colored as in *A*.

switching (*SI Appendix*, Fig. S6). However, as for curvature, I85L retains more WT-like switching characteristics in the pH data than LLL. Together, the pH and temperature dependencies of chemical shifts give a rich view of a network of residues throughout the WT protein that participate in switching and how the switching is greatly diminished, though not completely obliterated, by conservative hydrophobic mutations.

Mutagenesis of Hydrophobic Residues Reveals a Fine Balance in pH Switching. In order to better understand the large impacts of hydrophobic residues on the pH dependence of hisactophilin function, we used chemical denaturation to measure global energetics of switching for an extended set of mutants (Fig. 5). These mutants were chosen based on previous coarse-grained simulations and experiments which implicated the mutated residues in switching and include mutations affecting different regions of the β-barrel (13). Intriguingly, combining I85L with F6L restores the broken switch of I85 to a near-WT value of ΔG_{Switch} (Fig. 5*B*). Concurrently, there is an increase in stabilization upon myristoylation at low and high pH levels (Fig. 5*A*). These results support our previous proposal that the I85L mutation sterically blocks access of the myristoyl to the sequestered state (13) and indicate F6L may relieve putative steric strain to again allow myristoyl sequestration. Notably, another conservative change in stereochemistry, adding I93L to I85L/F6L (resulting in LLL), again breaks switching, this time with increased myristoyl stabilization hardly modulated by pH. This is consistent with a loss of protein populating the modestly stabilized accessible state. Unexpectedly, we found truncations of surface hydrophobic groups, I118A and I116A, also break switching, such that myristoylation confers little stabilization, comparable to I85L. In contrast, truncation of three hydrophobic residues in the protein core—F6L, V36A, and L76A—diminish pH switching while increasing stabilization by the myristoyl. This increased stabilization again points to the presence of strain or instability in the WT protein, proposed previously based on increased global protein folding dynamics caused by myristoylation (12). Such strain may be a feature of the core characteristics necessary to allow for two different myristoyl states. It is notable that many of the mutations that impair switching alter β-branched

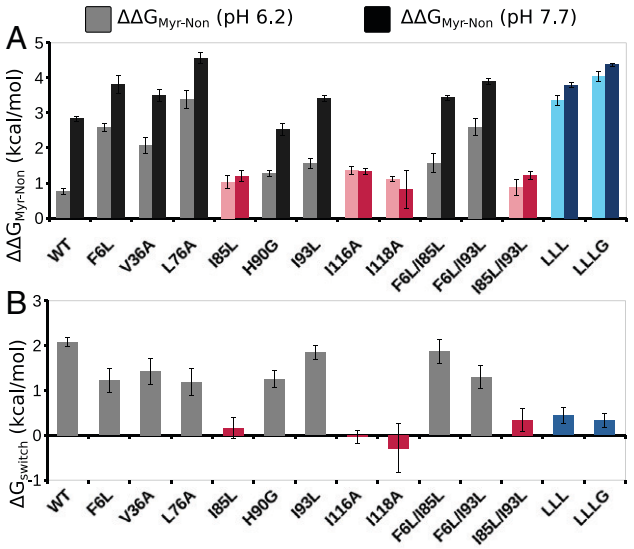

Fig. 5. Impacts of mutations on the global energetics of switching. (*A*) Change in global protein stability measured by chemical denaturation for myristoylated relative to nonmyristoylated mutant hisactophilins at pH 6.2 (light bars) and pH 7.7 (dark bars), $\Delta\Delta G_{Myr-Non} = \Delta G_{U-F,Myr} - \Delta G_{U-F,Non}$ in kilocalories per mole. Positive values of $\Delta\Delta G_{Myr-Non}$ indicate increased stability upon myristoylation. Gray or black indicates variants that can undergo switching. Red indicates variants that primarily populate the accessible state, as myristoylation is only modestly stabilizing at both pH levels, similar to the stabilization of WT at pH 6.2. Blue indicates a variant that predominantly populates the sequestered state, as myristoylation is strongly stabilizing at both pH levels, similar to WT at pH 7.7. Error bars represent the error in $\Delta\Delta G_{Myr-Non}$ calculated from the relative error of the fit of C_{mid} (the midpoint of denaturation). (*B*) Free energy of switching (if possible) is the difference in myristoyl stabilization at pH 7.7 relative to pH 6.2, $\Delta G_{Switch} = \Delta\Delta G_{Myr-Non,pH7.7} - \Delta\Delta G_{Myr-Non,pH6.2}$. The color scheme is the same as described in *A*. Plotted values and error bars are from fitting denaturation curve data to a binomial extrapolation model (*SI Appendix*, Tables S4–S6 and *Supplementary Methods*).

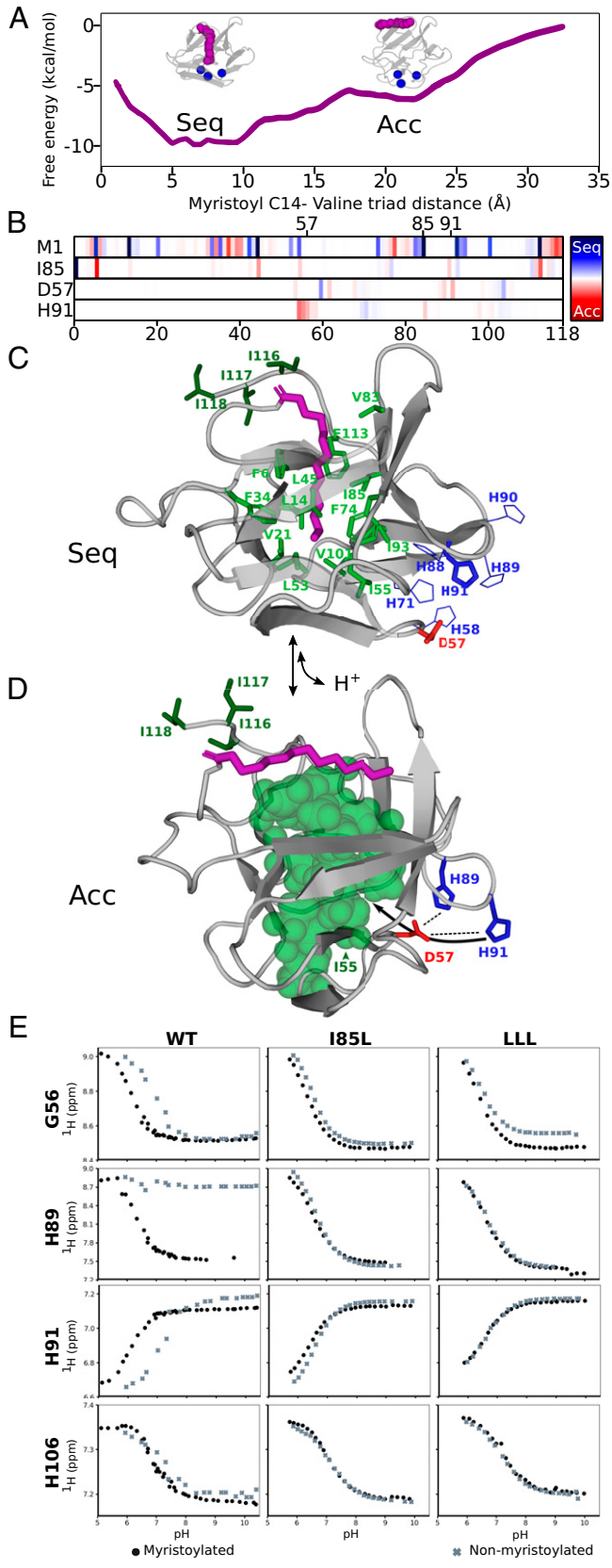

Fig. 6. Mechanism of pH-myristoyl switching in hisactophilin. (*A*) Umbrella sampling MD free-energy profile as a function of distance from the myristoyl (magenta spheres) C13 and C14 atom center of mass to the α carbon of the 3V center of mass (blue spheres). (*B*) Selected residues exhibiting pronounced changes in intermolecular contacts in the accessible state (C14-3V distance of 21 to 25 Å) relative to the sequestered state (C14-3V distance of 5 to 8 Å) in GBSW simulations at pH 6. In the strip for each residue, contacts are shown for myristoyl as residue 1 (M1) to I118 at the C terminus. The red-blue scale represents the change in contact formation spanning ±0.75; i.e., red indicates a contact was formed up to 75% more frequently in the accessible state (*SI Appendix*, Tables S7–S13; full contact plot in *SI Appendix*, Fig. S10). (*C*) Representative sequestered structure from GBSW simulations. The myristoyl (purple sticks) makes extensive contacts with hydrophobic core residues (green sticks). In the accessible state (*D*), core residues (filled green space) contact each other more frequently in the collapsed core, while the myristoyl makes contacts with residues at the top of the protein, including C-terminal I116, I117, and I118 (dark green). In GBSW simulations, the accessible state has increased favorable electrostatic interactions (dashed lines) of D57 with H91 and H89 (sticks); in the sequestered state, decreased contact with D57 and the many nearby histidines (thin blue lines) may contribute to decreased pK_{app} of H91. (*E*) Chemical shift versus pH for backbone amide protons of G56, H89, H91, and H106 in myristoylated(.) and nonmyristoylated(x) WT, I85L, and LLL. The stark change in pK_{app} of H91 and G56 in myristoylated versus nonmyristoylated WT is much decreased in the broken-switch mutants. In contrast, the fully solvent-exposed H106 is little affected by myristoylation or mutation.

residues, suggesting that steric constraints are also important. Taken together, the mutations studied affect switching in diverse ways—requiring a fine balance without one stable solution to make a myristoyl switch.

Hydrophobic-Electrostatic Switching Mechanism in Hisactophilin. Lastly, we conducted molecular dynamics (MD) simulations of hisactophilin using umbrella sampling with an explicit solvent and an implicit solvent generalized Born model with simple switching function (GBSW) at pH 6, 7, and 8; the MD results provide an atomistic view of switching that enabled a deeper interpretation and integration of the experimental data for WT and variant hisactophilins. Importantly, umbrella sampling MD with an explicit solvent identified two local energy minima at different locations for the myristoyl in WT hisactophilin. These energy minima are consistent with two preferred states, sequestered and accessible, and align with relative stabilities from chemical denaturation experiments (Figs. 5 and 6*A*). The GBSW simulations also found similar preferred locations (*SI Appendix*, Fig. S7). We define the sequestered state as corresponding to conformers where the C14 of the myristoyl is 5 to 8 Å from the centroid of V21, V61, and V101 (3V) at the bottom of the myristoyl binding pocket in the hisactophilin core, while in the accessible state, the C14 is 21 to 25 Å from 3V. Furthermore, GBSW MD showed a statistically significant increased population of sequestered relative to accessible conformations from pH 6 to 8 (*SI Appendix*, Fig. S7), which while much smaller, follows the same trend as experiments. The smaller pH dependence is not surprising given the GBSW model lacks a solvent dispersion term that would further stabilize the accessible state (35).

More detailed analysis of the simulations revealed structural features of switching. In the sequestered state, the myristoyl tends to be more extended than previously noted (13) (*SI Appendix*, Figs. S8 and S9) and is deeply buried, contacting hydrophobic residues right through the hisactophilin core (Fig. 6 *B* and C and *SI Appendix*, Fig. S10). Interestingly, in the accessible state, the myristoyl is also generally extended (*SI Appendix*, Figs. S8 and S9), laying across the top of the protein (Fig. 6*D*), where it samples many positions. These results may give insight into hisactophilin function, as in the accessible state, the myristoyl is positioned to easily interact with and insert into the cell membrane, a reversible phenomenon that occurs in vivo in chemotaxis and osmotic stress (8). Despite the much altered location of the myristoyl, the overall structure of hisactophilin is maintained upon switching, consistent with previous circular dichroism and NMR experiments (3). Thus, maintaining the protein fold may favor its function in rapid and reversible anchoring of actin to the cell membrane (3, 4). Compelling support for a lack of structural change upon membrane association

was obtained by encapsulating hisactophilin in reverse micelles, which provide a model of membrane binding (36). The spectrum for myristoylated hisactophilin undergoes extensive change upon encapsulation, becoming remarkably similar to the nonmyristoylated spectrum (*SI Appendix*, Fig. S11). These results are in agreement with the nonmyristoylated protein resembling the accessible state, being well folded and binding ready.

Further examination of intramolecular contacts identified another notable feature of the accessible state: prominent nonnative interactions of the myristoyl with hisactophilin's hydrophobic C-terminal residues I116, I117, and I118, which are much decreased in the sequestered state (Fig. 6*B*). The observation of these interactions by MD adds to earlier coarse-grained simulations where nonnative interactions were reported as essential for switching but not defined in detail (13). Importantly, this also provides insight on the loss of switching observed experimentally for I116A and I118A (Fig. 5). Further analyses of side-chain and main-chain contacts of I116 to I118 with the myristoyl show that side-chain interactions are also notably frequent when the myristoyl is positioned between accessible and sequestered (*SI Appendix*, Fig. S12). Also, β hairpin and β strand contacts in the N- and C-terminal regions are increased in the sequestered state, while the β4-β5 hairpin has increased contacts in the accessible state (*SI Appendix*, Fig. S10). Mutations of I to A typically decrease β structure propensity and thus may weaken contacts that stabilize the sequestered state. Together, these results implicate shifting interactions involving the C terminus as central to switching.

Finally, deeper analyses of contacts synergistic with experimental results at last provide strong evidence for key electrostatic participants in the switching mechanism. Overall, differences in contacts between sequestered and accessible conformations include a great many small changes throughout the protein, which are evident from simulations at all pH values (*SI Appendix*, Fig. S10 and Tables S7–S15). This is consistent with the involvement of the whole protein in switching, as observed by NMR. When ranking the contact differences between accessible conformations at pH 6 and sequestered conformations at pH 8 according to their magnitude (*SI Appendix*, Table S14), the largest increase in a favorable electrostatic contact occurs for D57 and H91 and a smaller increase occurs for D57 and H89 (Fig. 6*B* and *SI Appendix*, Fig. S10, respectively). Favorable electrostatic interactions of a carboxyl group with a histidine will enhance histidine protonation and thus increase its pK_a (28), as is clearly evident in the pK_{app} values for H91 and H89 in WT (Fig. 6*E*). As noted above, these changes are much diminished in the broken-switch mutants I85L and LLL, further supporting the mechanistic importance of these interactions in myristoyl switching (*SI Appendix*, Fig. S6). While NMR assignments are not available for D57, G56 and I55 exhibit pK_{app} behavior similar to that of H91, along with notably increased contacts with H91 (Fig. 6 *B* and *D* and *SI Appendix*, Fig. S10), indicating their close proximity.

The aforementioned electrostatic changes are accompanied by changes in a network of hydrophobic contacts. In the accessible state, increased interactions of H91 with residues I55 and I85 suggest H91 moves into a shallow hydrophobic pocket (Fig. 6 *B* and *D*). This pocket connects to the core of hisactophilin, where many hydrophobic residues have increased contacts (e.g., I85) (Fig. 6 *B* and *D* and *SI Appendix*, Fig. S10 and Tables S7–S15). The contact changes agree with trends toward the decreased radius of gyration for the β-barrel and the whole protein upon switching from sequestered to accessible (*SI Appendix*, Fig. S7). Together, these rearrangements may better position H91 and decrease solvent accessibility, thereby promoting H91-D57 interaction.

In the sequestered state, a decreased pK_{app} of ∼6 for H91 may be explained by loss of the favorable D57 interaction, along with increased electrostatic repulsion with multiple nearby histidines (H58, H71, H88, H89, and H90) (Fig. 6*C*). This raises the question of just how many histidines may participate in protonation changes during switching, noting that histidines are also thought to make favorable electrostatic interactions in membrane and actin binding by hisactophilin (4). The modest impairment of myristoyl switching in the H90G mutant (Fig. 5) shows this residue does not play a primary role in switching. The mutation is in a tight turn, where G is structurally favorable (37) and significantly stabilizes both the myristoylated and nonmyristoylated protein (Fig. 5*A* and *SI Appendix*, Table S6). The turn is flanked by the strands containing I85 and I93, which have key roles in switching. Thus, mutation to G may limit switching by decreasing requisite protein flexibility and diminishing electrostatic repulsion required for the decreased pK_{app} in the sequestered state. While H90 and other nearby histidines (H88, H71, and H58) do not exhibit substantial changes in electrostatic contacts associated with switching, H89 may well cooperate with H91 such that their combined molecular ionization is a major driver of switching (38).

It should be noted that many residues exhibit a pK_{app} of ∼6 in myristoylated hisactophilin (*SI Appendix*, Fig. S6), which may further reflect molecular ionization, as well as coordinated conformational changes in switching. Additional minor contributors to switching may include increased favorable electrostatic interaction of H9 and E114, similar to but less pronounced than H91 and D57 in chemical shift and contact changes (*SI Appendix*, Fig S10 and Tables S7–S15). There are also other small changes in contacts for pairs of histidine residues (*SI Appendix*, Tables S7–S15). Taken together, the simulation results explain previous experimental results, and vice versa, revealing how electrostatic interactions, in concert with a network of hydrophobic interactions, toggle switching.

Myristoyl Switch Mechanisms. In this study, we present NMR, mutagenesis, and MD results that provide high-resolution insights into the allosteric mechanism of pH-myristoyl switching in hisactophilin. Simulation reveals details of the change in the myristoyl environment during switching, from its sequestration deep in the protein hydrophobic core to being closer to the surface of the protein, where it interacts weakly with the hydrophobic C terminus and is available to insert into the membrane. Upon emergence of the myristoyl, a network of increased hydrophobic interactions and contraction of the core occur, along with the formation of key favorable electrostatic interactions on the protein surface. The computational results mirror the temperature, pH, and mutagenesis dependence of NMR data and global protein switching measured by chemical denaturation. Thus, a coherent, high-resolution view emerges of an integrated, proteinwide response.

The pH-myristoyl switching mechanism in hisactophilin presents an interesting case study of coupled core hydrophobic-surface electrostatic allostery. In comparison, myristoyl switching of recoverin, as part of light signal transduction in the retina, is regulated by calcium binding, which causes the myristoyl to switch from being buried in the core of this helical protein to solvent exposed, accompanied by large conformational changes around a pivot point between the two EF-hand domains (5). Myristoyl switching of the HIV-1 MA protein results in more limited but significant structural changes (36). In contrast, hisactophilin switching causes little change to the native fold (12), which may facilitate rapid and reversible membrane and actin binding functions. Hisactophilin may have a dynamic aspect to its

switching, akin to a guanine cyclase-activating protein, GCAP, where myristoyl switching does not change structure, instead causing large changes in protein dynamics (39, 40). Myristoylation of hisactophilin accelerates its global protein folding and unfolding kinetics, which together with rapid switch kinetics and a binding pocket smaller than the myristoyl group, suggested strain in native hisactophilin as a likely feature of switching (12, 13). The increased stabilization upon myristoylation observed here for truncation- and stereochemistry-changing hydrophobic mutants compared to WT further supports the presence of strain in native hisactophilin. Strain may be considered in terms of a balance or metastability between the sequestered and the accessible states, with the temperature and pH dependence of amide chemical shifts suggesting intricate trade-offs in stability at the local level. These trade-offs change with pH or mutation to alter the relative global energies of the two states and thus favor the population of one state or the other (Figs. 5 and 6*A*).

Allosteric control of protein function via protonation is widespread—occurring, e.g., in many actin-regulatory proteins, pathogenic proteins, and hemoglobin—but is perhaps underrecognized (41, 42). The increased use of constant-pH and pH-replica exchange MD simulations has enabled the study of many pH-dependent allosteric mechanisms (42–44) but has not before been applied to proteins with as many ionizable residues as hisactophilin. Accordingly, the methods demonstrated here for hisactophilin could be applied to other proteins and their variants to elucidate regulation by binding of protons or a variety of other possible ligands, and they may be particularly advantageous for those demonstrating complex and widely distributed allosteric networks.

Amide Temperature-Dependent Differences for Determining Interaction Networks in Proteins. Differences in the temperature dependence of amide chemical shifts are demonstrating increasing promise as a valuable expansion of the NMR toolkit for protein characterization. The example of hisactophilin illustrates the information-rich results and high sensitivity afforded by amide temperature dependencies to define interaction networks and the population of alternative states. Another advantage is the ease of acquiring and analyzing the results. Linear TCs are well established as reporting on hydrogen bonding in proteins (6, 14, 15, 21, 27, 45–47). Furthermore, TCs may report more generally on the temperature-dependent loss of structure (16). Notably, TC comparisons of mutant proteins revealed distinct networks of local stability perturbations, which were consistent with structural changes observed by crystallography and not limited to changes in hydrogen bonding, while summed TCs agreed well with measurements of global stability by calorimetry (17, 18).

It is important to note that while more negative TCs are typically observed for amides in mobile loops compared to those in a stable secondary structure (relating to inter- versus intramolecular hydrogen bonding changes with temperature, respectively) (14, 15, 29, 48), TCs cannot be interpreted quantitatively in terms of absolute local stability owing to the many factors that can influence amide chemical shifts. For the same reason, a lack of curvature does not prove a lack of conformational heterogeneity (31, 49). However, analyzing the differences between related protein variants or solution conditions allows the effects of the variation to be discerned by eliminating many unrelated effects on chemical shifts. Thus, surface residues in hisactophilin, including histidines, generally show less change associated with myristoyl switching (*SI Appendix*, Tables S2 and S3). Even more compelling is the lack of changes in the broken-switch mutants. Notably, for WT, the largest changes in temperature dependencies associated with switching tend to be observed for residues that global stability measurements also show are important in switching (Fig. 5). The temperature dependence analyses may nevertheless underestimate the residues involved in the network because their chemical shift changes associated with switching may be small. A TC cycle analysis of coupling between interacting groups may in principle be applied using variants with different combinations of interacting groups, such as posttranslational modification (e.g., myristoyl, phosphoryl, and acetyl), bound ligand (H^+, Ca^{2+}, and peptides), and mutation. Thus, a conservative interpretation of TC changes, including many amides, can provide another valuable tool for identifying interaction networks and allosteric coupling.

In conclusion, we demonstrate here how measurements of amide proton temperature dependence of chemical shifts provide a rich and sensitive view of allostery, linking the hisactophilin hydrophobic core to surface electrostatics. The view from MD simulations is strongly consistent and synergistic with experiments. Exploiting underexplored chemical shift differences and cycle analyses may provide high-resolution insights for many systems, including a wide variety of proteins and peptide assemblies (16, 21–26), and serve as a valuable resource to complement, test, and refine molecular simulations.

Materials and Methods

Details of all methods are described in *SI Appendix*.

Protein Expression and Purification. Hisactophilin was expressed as previously described (12) in *Escherichia coli* BL21 cells. Protein for NMR experiments was expressed in minimal media with $^{15}NH_4Cl$. Protein was purified with immobilized metal affinity chromatography, followed by acetonitrile gradient reversed-phase high-pressure liquid chromatography to separate myristoylated and nonmyristoylated forms (13).

Variable-Temperature NMR Experiments. Hisactophilin labeled with ^{15}N was prepared in 50 mM phosphate buffer (pH 7.7) or 50 mM 2-(*N*-morpholino)ethanesulfonic acid buffer (pH 6.2), also containing 1 mM ethylenediaminetetraacetic acid, 1 mM dithiothreitol, 10% deuterium oxide, and 1 mM 4,4-dimethyl-4-siapentane-1-sulfonic acid (DSS). ^1H-^{15}N HSQC spectra were acquired from 278 to 318 K in 5-K increments for WT hisactophilin and from 283 to 323 K using 2.5-K increments for hisactophilin mutants on a Bruker Avance 600-MHz spectrometer. Chemical shifts were referenced using DSS as described previously (18). Separation of the water and DSS peaks was used as an internal thermometer to determine the actual temperature for each increment. Assignments were obtained as described in *SI Appendix*. TC values were determined by least-squares linear regression of ^1H chemical shift values versus temperature (17). Deviations from linearity (curvature) of the temperature dependencies were identified by subtracting the line of best fit from the observed chemical shifts, and the fit of residual chemical shifts to linear and second-order polynomial regressions was compared with a bootstrapped *F* test. Temperature dependencies were considered curved when the quadratic coefficient differed from zero at $P < 0.01$.

NMR-Monitored pH Titrations. Hisactophilin was prepared in the same phosphate buffer as above, except with an initial pH of 10. The pH was adjusted down to ∼pH 5.80 in pH 0.1- to 0.2-unit steps using hydrochloric acid, and a one-dimensional ^1H spectrum and two-dimensional ^1H-^{15}N HSQC were acquired at each step. Analysis was completed using CCPN version 2.4 (Collaborative Computing Project for NMR) (50).

Chemical Denaturation. Equilibrium urea denaturation monitored by tyrosine fluorescence was performed as described previously (29) at pH 6.2 and 7.7.

Encapsulation in Reverse Micelles. Hisactophilin was encapsulated in a cetyltrimethylammonium bromide:hexanol reverse micelle with a pH 8.1 or 6.1 aqueous interior (36). ^1H-^{15}N HSQC spectra were obtained on a 500-MHz Bruker spectrometer.

Umbrella Sampling MD Simulations. The starting structure was based on an NMR structure (Protein Data Bank [PDB]: 1HCD) with a myristoyl modeled in

based on nuclear Overhauser effect (NOE) restraints (12). Simulations were performed with the Nanoscale Molecular Dynamics (NAMD) package using the TIP3P water model and AMBER03 force field. The myristoyl depths measured between the geometric centers of the myristoyl C13-C14 atoms and the Cα atoms of 3V were divided into 0.5-Å windows from 1 to 32.5 Å. After initial minimization and equilibration, 60 ns of production simulation time (on average) was performed for each umbrella sampling window for a total simulation time of more than 3,000 ns.

Implicit Solvent GBSW MD Simulations. Simulations were performed using the Chemistry at Harvard Macromolecular Mechanics (CHARMM) package and the CHARMM22 force field with the implicit solvent constant pH molecular dynamics (CpHMD) algorithm, implemented as previously described (51), and an implicit solvent GBSW model (52). Patches on titratable groups ASP, GLU, and HIS were applied to the same starting structure as above, followed by minimization. The 100 replicate 20-nm simulations were performed at pH 6, 7, and 8.

Data Availability. Amide backbone chemical shift assignments have been deposited to the BMRB for wild-type (deposition nos. 51280, 51271, 51269, 51270), LLL (51276, 51275, 51277, 51274), and I85L (51278, 51273, 51279, 51272) hisactophilin under each of the following conditions, respectively: nonmyristoylated pH 6.2, nonmyristoylated pH 7.7, myristoylated pH 6.2, and myristoylated pH 7.7. All other study data are included in the article and/or *SI Appendix*.

ACKNOWLEDGMENTS. We thank Jan Venne and Dr. Kathy Valentine for their assistance with NMR experiments at the University of Waterloo and the University of Pennsylvania, respectively. We also thank Dr. Hedieh Torabifard for her assistance with implicit solvent simulations and Colleen Doyle for her generous insights. We acknowledge funding from Natural Sciences and Engineering Research Council (NSERC) of Canada Discovery Grant and Compute Canada to E.M.M.; the University of Pennsylvania Research Fund and NIH R21CA206958 to A.J.W.; NIH GM130587 and GM107233 to C.L.B.; NSERC Collaborative Research and Training Experience funds to D.N. and J.S.; NSERC Canada Graduate Scholarship to A.S. and J.S.; NSERC Postgraduate Scholarship to D.W.S.M.; NSERC Undergraduate Student Research Assistantship to A.S., J.S., and C.A.L.; and Ontario Graduate Scholarship to A.S., J.S., D.N., A.B., and M.T.J.S.

Author affiliations: [a]Department of Chemistry, University of Waterloo, Waterloo, ON N2L 3G1, Canada; [b]Department of Chemistry and Biophysics, University of Michigan, Ann Arbor, MI 48109; and [c]Department of Biochemistry and Biophysics, Perelman School of Medicine, University of Pennsylvania, Philadelphia, PA 19104

Author contributions: D.W.S.M. and E.M.M. designed research framework; D.W.S.M., M.T.J.S., B.F., A.J.W., and E.M.M. designed NMR experiments; D.W.S.M., D.N., T.K., P.S., M.Q.N., E.T., M.T.J.S., and B.F. performed NMR and chemical denaturation experiments; E.A., A.B., and C.L.B. designed and performed computational experiments; D.W.S.M., A.S., J.S., C.A.L., M.T.J.S., and E.M.M. analyzed data; A.S., J.S., D.N., and E.M.M. wrote the paper, in consultation with D.W.S.M., C.A.L., A.B., M.T.J.S., B.F., A.J.W., and C.L.B.

1. S. J. Wodak *et al.*, Allostery in its many disguises: From theory to applications. *Structure* **27**, 566–578 (2019).
2. H. N. Motlagh, J. O. Wrabl, J. Li, V. J. Hilser, The ensemble nature of allostery. *Nature* **508**, 331–339 (2014).
3. F. Hanakam, R. Albrecht, C. Eckerskorn, M. Matzner, G. Gerisch, Myristoylated and non-myristoylated forms of the pH sensor protein hisactophilin II: Intracellular shuttling to plasma membrane and nucleus monitored in real time by a fusion with green fluorescent protein. *EMBO J.* **15**, 2935–2943 (1996).
4. F. Hanakam, G. Gerisch, S. Lotz, T. Alt, A. Seelig, Binding of hisactophilin I and II to lipid membranes is controlled by a pH-dependent myristoyl-histidine switch. *Biochemistry* **35**, 11036–11044 (1996).
5. J. B. Ames, T. Tanaka, L. Stryer, M. Ikura, Portrait of a myristoyl switch protein. *Curr. Opin. Struct. Biol.* **6**, 432–438 (1996).
6. K. Chandra, Y. Sharma, K. V. R. Chary, Characterization of low-energy excited states in the native state ensemble of non-myristoylated and myristoylated neuronal calcium sensor-1. *Biochim. Biophys. Acta* **1814**, 334–344 (2011).
7. S. McLaughlin, A. Aderem, The myristoyl-electrostatic switch: A modulator of reversible protein-membrane interactions. *Trends Biochem. Sci.* **20**, 272–276 (1995).
8. T. Pintsch, H. Zischka, S. C. Schuster, Hisactophilin is involved in osmoprotection in Dictyostelium. *BMC Biochem.* **3**, 10 (2002).
9. M. D. Resh, Fatty acylation of proteins: The long and the short of it. *Prog. Lipid Res.* **63**, 120–131 (2016).
10. M. M. Attwood, D. Fabbro, A. V. Sokolov, S. Knapp, H. B. Schiöth, Trends in kinase drug discovery: Targets, indications and inhibitor design. *Nat. Rev. Drug Discov.* **20**, 839–861 (2021).
11. F. J. Adrián *et al.*, Allosteric inhibitors of Bcr-abl-dependent cell proliferation. *Nat. Chem. Biol.* **2**, 95–102 (2006).
12. M. T. Smith, J. Meissner, S. Esmonde, H. J. Wong, E. M. Meiering, Energetics and mechanisms of folding and flipping the myristoyl switch in the beta-trefoil protein, hisactophilin. *Proc. Natl. Acad. Sci. U.S.A.* **107**, 20952–20957 (2010).
13. D. Shental-Bechor *et al.*, Nonnative interactions regulate folding and switching of myristoylated protein. *Proc. Natl. Acad. Sci. U.S.A.* **109**, 17839–17844 (2012).
14. T. Cierpicki, J. Otlewski, Amide proton temperature coefficients as hydrogen bond indicators in proteins. *J. Biomol. NMR* **21**, 249–261 (2001).
15. T. Cierpicki, J. Otlewski, NMR structures of two variants of bovine pancreatic trypsin inhibitor (BPTI) reveal unexpected influence of mutations on protein structure and stability. *J. Mol. Biol.* **321**, 647–658 (2002).
16. J. H. Tomlinson, M. P. Williamson, Amide temperature coefficients in the protein G B1 domain. *J. Biomol. NMR* **52**, 57–64 (2012).
17. C. M. Doyle *et al.*, Concurrent Increases and decreases in local stability and conformational heterogeneity in Cu, Zn superoxide dismutase variants revealed by temperature-dependence of amide chemical shifts. *Biochemistry* **55**, 1346–1361 (2016).
18. K. Trainor, J. A. Palumbo, D. W. S. MacKenzie, E. M. Meiering, Temperature dependence of NMR chemical shifts: Tracking and statistical analysis. *Protein Sci.* **29**, 306–314 (2020).
19. J. E. Dawson *et al.*, Non-cooperative 4E-BP2 folding with exchange between eIF4E-binding and binding-incompatible states tunes cap-dependent translation inhibition. *Nat. Commun.* **11**, 3146 (2020).
20. M. Kim *et al.*, Evidence that the TRPV1 S1-S4 membrane domain contributes to thermosensing. *Nat. Commun.* **11**, 4169 (2020).
21. G. P. Lisi, A. A. Currier, J. P. Loria, Glutamine hydrolysis by imidazole glycerol phosphate synthase displays temperature dependent allosteric activation. *Front. Mol. Biosci.* **5**, 4 (2018).
22. H. Launay *et al.*, Flexibility of oxidized and reduced states of the chloroplast regulatory protein CP12 in isolation and in cell extracts. *Biomolecules* **11**, 701 (2021).
23. M. Dellarole *et al.*, Evolutionarily conserved pattern of interactions in a protein revealed by local thermal expansion properties. *J. Am. Chem. Soc.* **137**, 9354–9362 (2015).
24. K. S. Chatterjee, D. S. S. Hembram, R. Das, Amide temperature coefficients in characterizing the allosteric effects of ligand binding on local stability in proteins. *Biochem. Biophys. Res. Commun.* **524**, 677–682 (2020).
25. S. H. Bhate, J. B. Udgaonkar, R. Das, Destabilization of polar interactions in the prion protein triggers misfolding and oligomerization. *Protein Sci.* **30**, 2258–2271 (2021).
26. H. V. Schröder, Y. Zhang, A. J. Link, Dynamic covalent self-assembly of mechanically interlocked molecules solely made from peptides. *Nat. Chem.* **13**, 850–857 (2021).
27. N. J. Baxter, M. P. Williamson, Temperature dependence of 1H chemical shifts in proteins. *J. Biomol. NMR* **9**, 359–369 (1997).
28. A. Fersht, *Structure and Mechanism in Protein Science* (Freeman, 1999).
29. H. J. Wong, P. B. Stathopulos, J. M. Bonner, M. Sawyer, E. M. Meiering, Non-linear effects of temperature and urea on the thermodynamics and kinetics of folding and unfolding of hisactophilin. *J. Mol. Biol.* **344**, 1089–1107 (2004).
30. M. T. J. Smith, D. W. S. Mackenzie, E. M. Meiering, Dissecting the molecular determinants of ligand-binding-induced macromolecular switching using thermodynamic cycles. *Protein Eng. Des. Sel.* **24**, 213–217 (2011).
31. N. J. Baxter, L. L. Hosszu, J. P. Waltho, M. P. Williamson, Characterisation of low free-energy excited states of folded proteins. *J. Mol. Biol.* **284**, 1625–1639 (1998).
32. R. B. Tunnicliffe, J. L. Waby, R. J. Williams, M. P. Williamson, An experimental investigation of conformational fluctuations in proteins G and L. *Structure* **13**, 1677–1684 (2005).
33. M. P. Williamson, Many residues in cytochrome c populate alternative states under equilibrium conditions. *Proteins* **53**, 731–739 (2003).
34. A. K. Srivastava, K. V. R. Chary, Conformational heterogeneity and dynamics in a βγ-crystallin from Hahella chejuensis. *Biophys. Chem.* **157**, 7–15 (2011).
35. J. Chen, C. L. Brooks, 3rd, Implicit modeling of nonpolar solvation for simulating protein folding and conformational transitions. *Phys. Chem. Chem. Phys.* **10**, 471–481 (2008).
36. K. G. Valentine *et al.*, Reverse micelle encapsulation of membrane-anchored proteins for solution NMR studies. *Structure* **18**, 9–16 (2010).
37. A. M. C. Marcelino, L. M. Gierasch, Roles of beta-turns in protein folding: from peptide models to protein engineering. *Biopolymers* **89**, 380–391 (2008).
38. D. Bashford, M. Karplus, pKa's of ionizable groups in proteins: Atomic detail from a continuum electrostatic model. *Biochemistry* **29**, 10219–10225 (1990).
39. I. V. Peshenko, E. V. Olshevskaya, S. Lim, J. B. Ames, A. M. Dizhoor, Calcium-myristoyl Tug is a new mechanism for intramolecular tuning of calcium sensitivity and target enzyme interaction for guanylyl cyclase-activating protein 1: Dynamic connection between N-fatty acyl group and EF-hand controls calcium sensitivity. *J. Biol. Chem.* **287**, 13972–13984 (2012).
40. T. Orban *et al.*, Conformational changes in guanylate cyclase-activating protein 1 induced by Ca2+ and N-terminal fatty acid acylation. *Structure* **18**, 116–126 (2010).
41. A. Schönichen, B. A. Webb, M. P. Jacobson, D. L. Barber, Considering protonation as a posttranslational modification regulating protein structure and function. *Annu. Rev. Biophys.* **42**, 289–314 (2013).
42. A. Kumawat, S. Chakrabarty, Protonation-induced dynamic allostery in PDZ domain: Evidence of perturbation-independent universal response network. *J. Phys. Chem. Lett.* **11**, 9026–9031 (2020).
43. R. C. Harris, C.-C. Tsai, C. R. Ellis, J. Shen, Proton-coupled conformational allostery modulates the inhibitor selectivity for β-secretase. *J. Phys. Chem. Lett.* **8**, 4832–4837 (2017).
44. N. V. Di Russo, M. A. Martí, A. E. Roitberg, Underlying thermodynamics of pH-dependent allostery. *J. Phys. Chem. B* **118**, 12818–12826 (2014).
45. A. Sekhar *et al.*, Thermal fluctuations of immature SOD1 lead to separate folding and misfolding pathways. *eLife* **4**, e07296 (2015).
46. M. Kjaergaard *et al.*, Temperature-dependent structural changes in intrinsically disordered proteins: Formation of α-helices or loss of polyproline II? *Protein Sci.* **19**, 1555–1564 (2010).
47. G. Bouvignies, P. Vallurupalli, M. H. J. Cordes, D. F. Hansen, L. E. Kay, Measuring 1HN temperature coefficients in invisible protein states by relaxation dispersion NMR spectroscopy. *J. Biomol. NMR* **50**, 13–18 (2011).
48. N. H. Andersen *et al.*, Extracting information from the temperature gradients of polypeptide NH chemical shifts 1. The importance of conformational averaging. *J. Am. Chem. Soc.* **119**, 8547–8561 (1997).
49. S. Yao, I. G. Young, R. S. Norton, J. M. Murphy, Murine interleukin-3: Structure, dynamics, and conformational heterogeneity in solution. *Biochemistry* **50**, 2464–2477 (2011).
50. W. F. Vranken *et al.*, The CCPN data model for NMR spectroscopy: Development of a software pipeline. *Proteins* **59**, 687–696 (2005).
51. E. J. Arthur, C. L. Brooks 3rd, Efficient implementation of constant pH molecular dynamics on modern graphics processors. *J. Comput. Chem.* **37**, 2171–2180 (2016).
52. W. Im, M. S. Lee, C. L. Brooks 3rd, Generalized born model with a simple smoothing function. *J. Comput. Chem.* **24**, 1691–1702 (2003).